

Eckhaus instability in the Lugiato-Lefever model^{*}

Nicolas P erinet^{1,a}, Nicolas Verschueren², and Saliya Coulibaly³

¹ Departamento de F ısica, Facultad de ciencias F ısicas y Matem aticas, Universidad de Chile, 487-3 Casilla, Santiago, Chile

² Department of Engineering Mathematics, University of Bristol, Queen's Building, University Walk, Bristol BS8 1TR, UK

³ Laboratoire de Physique des Lasers, Atomes et Molecules, CNRS UMR 8523, Universit  des Sciences et Technologies de Lille, 59655 Villeneuve d'Ascq Cedex, France

Received 1 February 2017 / Received in final form 5 June 2017

Published online 26 September 2017 –   EDP Sciences, Societ  Italiana di Fisica, Springer-Verlag 2017

Abstract. We study theoretically the primary and secondary instabilities undergone by the stationary periodic patterns in the Lugiato-Lefever equation in the focusing regime. Direct numerical simulations in a one-dimensional periodic domain show discrete changes of the periodicity of the patterns emerging from unstable homogeneous steady states. Through continuation methods of the steady states we reveal that the system exhibits a set of wave instability branches. The organisation of these branches suggests the existence of an Eckhaus scenario, which is characterized in detail by means of the derivation of their amplitude equation in the weakly nonlinear regime. The continuation in the highly nonlinear regime shows that the furthest branches become unstable through a Hopf bifurcation.

1 Introduction

Nonlinear optics has become an active research field since the introduction of the laser in 1960, which gave rise to a great development of optical experimental instruments. In addition, devices including all types of fiber cavities [1], cavity metamaterials [2,3], Kerr optical frequency combs [4] and liquid crystals have a wide range of applications [5] extending from metrology to the storage or transmission of information. Generally speaking, theoretical modelling of most of these physical systems is a complicated task. A strategy to overcome this difficulty is to derive a reduced model that describes the original system [6]. The Lugiato-Lefever equation (LL) [7] belongs to this class of reduced models. It is the prototype model that accounts for the dynamics in an externally driven cavity composed of a medium with Kerr-type nonlinearity. A large variety of dissipative structures have been singled out or studied by means of the LL equation in many physical areas in both one- and two-dimensional systems. Examples include localised structures or cavity solitons [8], fronts [9] and periodic patterns [1,10,11]. In the one-dimensional case the homogeneous steady solution undergoes a Turing instability giving rise to periodic patterns. Near the threshold, the patterns are stationary and they can be approximated by the solution of the linearized equation [7]. Hence, the characteristic length scale of the pattern is well described

by means of the linear stability analysis of the homogeneous steady state. The dynamical evolution of these Turing rolls in the weakly nonlinear regime has been described by means of the Ginzburg-Landau equation, which exhibits Eckhaus instabilities [12]. The derivation of the amplitude equation relies on an effective separation of spatial scales. However, numerical simulations show that the periodicity provided by the linear stability analysis fails to describe the instability in a large region of the parameter space [13].

The aim of the present paper is to study one of the simplest aspects of this equation: the bifurcations of the stationary patterns in a one-dimensional periodic system. The investigation undertaken here is numerical and theoretical. The numerical tools used are continuation through direct numerical integration and pseudo arc-length continuation, which permits one to follow the integrity of a solution branch when one parameter is varied. Our numerical simulations suggest that the stationary patterns undergo abrupt changes of wavelength in the parameter space composed by the driving strength and the detuning. This phenomenon is called the Eckhaus instability [14]. Comparisons between both methods show an excellent agreement. By means of the normal form procedure, we derive a Ginzburg-Landau amplitude equation from the original LL model. Considering the amplitude equation obtained, we use the analysis described in [15] to predict the occurrences of the Eckhaus instability. Close to the primary instability, the theory predicts well the first few transitions.

The article is organised as follows. In Section 2, we give a short description of the LL equation and a summary

^{*} Contribution to the Topical Issue "Theory and Applications of the Lugiato-Lefever Equation", edited by Yanne K. Chembo, Damia Gomila, Mustapha Tlidi, Curtis R. Menyuk.

^a e-mail: nperinet@ing.uchile.cl

of the results obtained using analytical techniques. Section 3 is devoted to the numerical part of our study. We start the section with a description of the numerical methods used and then we study the dynamical evolution of the pattern when the detuning and injection parameters are varied. In both cases the Eckhaus instabilities are observed. In Section 4, we derive the normal form which allows us to predict the appearance and stabilization of the branches in the Eckhaus instability. Finally, in Section 5, concluding remarks and discussion of our results are provided.

2 The Lugiato-Lefever (LL) model

The Lugiato-Lefever model [7] is an equation widely used in nonlinear optics. It describes the spatio-temporal evolution of a complex field (an electric field in the optical context). This model is derived from the Maxwell-Bloch equations (used in bistable optical resonators) by using the mean field approximation, the adiabatic elimination of the atomic variables and the idealization of a purely dispersive medium (no absorption). The solutions of the LL model show remarkable agreement with the behaviour of light in many optical devices.

In one-dimensional systems, the LL equation reads as follows:

$$\partial_t \psi = -\psi + i\eta (|\psi|^2 - \theta) \psi + i\partial_{xx} \psi + F. \quad (1)$$

In an optical setting, the parameters θ and F are real and they represent the detuning and the amplitude of the light input field, respectively. The parameter η only takes the values ± 1 and accounts for a focusing (+1) or a defocusing (-1) nonlinearity. ψ stands for the slowly varying envelope of the electric field within the optical cavity. The variable t stands for the time and x for the spatial component. We restrict ourselves to the self-focusing case ($\eta = 1$), so that (1) becomes

$$\partial_t \psi = f(\psi; \theta, F) = -(1 + i\theta)\psi + i|\psi|^2\psi + i\partial_{xx}\psi + F. \quad (2)$$

Writing $\psi = R + iS$, equation (2) becomes

$$\begin{aligned} \partial_t R(x, t) &= -R + \theta S - (R^2 + S^2)S - \partial_{xx} S + F, \\ \partial_t S(x, t) &= -S - \theta R + (R^2 + S^2)R + \partial_{xx} R. \end{aligned} \quad (3)$$

Let ψ_h be a homogeneous steady solution of the LL equation. Then, setting $I_0 = |\psi_h|^2$ one has:

$$F = F_h = \sqrt{I_0 (1 + (\theta - I_0)^2)}, \quad (4)$$

and

$$R_h = \frac{F}{1 + (I_0 - \theta)^2}, \quad S_h = \frac{F(I_0 - \theta)}{1 + (I_0 - \theta)^2}. \quad (5)$$

It results from (4) that the number of branches of the bifurcation diagram of the homogeneous steady state is controlled by the detuning parameter θ . Indeed, for $\theta < \sqrt{3}$ ($\theta > \sqrt{3}$) the system is monostable (bistable).

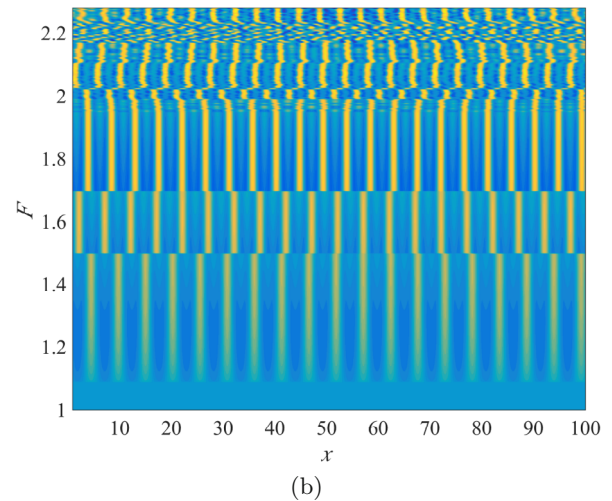
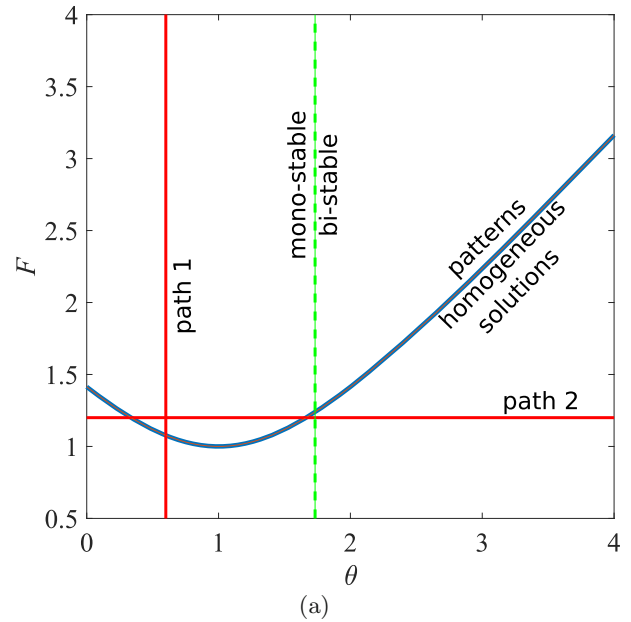


Fig. 1. (a) Domain of stability for steady solutions of the LL Model. On the right of the dashed line ($\theta = \sqrt{3}$) two stable solutions coexist. The parabola centered on $\theta = 1$ marks the locus where a spatial instability takes place. In the parameter subset lying over the parabola, spatially periodic patterns are observed. The red lines show the paths we chose to explore in the next sections, more precisely ($\theta = 0.6, F$) and ($\theta, F = 1.2$). (b) Contour plot of $|\psi(x, t_*)|$ at $t_* = 10000$ of the states observed from direct numerical integration in the space (horizontal line) over *path 1* as F (vertical axis) is increased.

Linear stability analysis of the solution ψ_h predicts the existence of a Turing instability with the critical wavenumber $k_c = \sqrt{2 - \theta}$ for $I_0 \equiv I_c = 1$. Consequently, the boundary between the stable and unstable regime is given by:

$$F^2 \equiv F_c^2(\theta) = \theta^2 - 2\theta + 2. \quad (6)$$

Figure 1a shows this separatrix in the plane (θ, F) . Along this curve, the marginal eigenmode can be written as:

$$\Psi_c = \mathbf{w} (Ae^{ik_c x} + c.c.), \quad (7)$$

where $\mathbf{w} = (\theta, 2 - \theta)^T$, A is an undetermined complex constant and the symbol *c.c.* stands for complex conjugate. The Turing instability is a codimension-one bifurcation which gives rise to the appearance of spatial patterns. Along the critical curve (6), there is a codimension-two point where the bifurcation for the amplitude A of the patterns changes from subcritical to supercritical. This point is found by means of an amplitude equation (see Sect. 4). In the subcritical case of the LL model two types of localised structures have been observed: localised patterns (homoclinic snaking) and soliton-like (single-peak) structures (see Refs. [16–19] for details).

In the following study of the LL model, we compare direct numerical simulations, continuation of the stationary solutions and analytical calculations obtained from the linear stability analysis and the amplitude equation. The linear stability analysis is a good tool to predict wavenumber selection at onset. Unfortunately, it fails to describe the wavelength selection far from the threshold. Here, we propose to follow this selection process in a large region of the parameter space. More specifically, we study the evolution of the patterns when F and θ are modified. For this purpose, we have chosen two paths displayed in Figure 1a: the *path 1* (*path 2*) which accounts for the evolution with respect to F (θ) for fixed θ (F).

The value $\theta = 0.6$ in *path 1* has been chosen so as to stay in the supercritical region ($\theta < 41/30$) where the amplitude equation is in quantitatively good agreement with the solution of (2) and then the comparison between the amplitude equation and the numerical observations can be performed (see Sect. 4). Moreover, since *path 1* is in the monostable and supercritical case, there are no other stable solutions to which the direct numerical simulation can converge and the computations can be easily reproduced.

For *path 2*, we fixed F at 1.2 in order to spot a sufficient number of interesting phenomena without being overloaded by data, since the number of stationary branches increases rapidly with F .

3 Numerical results

In general, the structure of the solutions of an evolution equation like (2) can be partly captured by studying its stationary version, which reduces to solving $f(\Psi; \theta, F) = 0$ in (2). The set of stationary solutions of (2) is sought by means of a continuation method described below. A preliminary direct numerical integration in the same range of parameters helps us to foresee the structure of these stationary solutions.

Numerical continuation methods are designed to follow a specific branch of solution over its whole range of existence, assuming that two points of the branch are already known. In this description, we assume F to be the control parameter while θ is fixed. The most successful method is called Predictor-Corrector pseudo arc-length continuation method (see for example [20] or [21]) and consists of two distinct steps. First, a predictor step estimates a new point of the branch in the (F, Ψ) space from existing points. Second, the estimation is refined through a corrector step where the stationary version of (2): $f(\Psi; \theta, F) = 0$ is trans-

formed into a system of algebraic equations using finite differentiation. The closure of the system, which also contains the control parameter as an unknown, is ensured by fixing a hyperplane in the parameter-phase space to which the direction of each correction step is restricted [21]. The algebraic system is then solved by means of a Newton-type method. In the case of large systems, matrix-free solvers can be used [22]. These methods do not require the explicit knowledge of the Jacobian matrix involved in the corrector step.

Continuation methods are in general more accurate and converge faster than direct integration. In addition, they compute unstable as well as stable solutions. The stability of a solution is accessible through the Jacobian matrix of f . While a branch is continued, the systematic application of simple criteria (see [23] for details) permits one to find and identify bifurcations or branching points. The direction of the new branches emerging from these points can be computed analytically in some cases [23] or by perturbing f near the bifurcation and switching back to the unperturbed f after the bifurcation is passed. Finally, note that numerical continuation methods do not only find equilibrium solutions, but also limit cycles, invariant tori [24] and heteroclinic orbits [25]. Numerous open source packages specialized in continuation have also been developed during the last decades (e.g. AUTO, MATCONT, COCO, pde2path).

The results obtained through the pseudo arc-length continuation are compared with direct numerical integrations. At each increment of the control parameter, the final solution at the previous value of the parameter is taken as the initial condition for the new computation. In this way the solution stays on the same branch until it becomes unstable.

For our model, we have developed direct numerical integration and continuation codes. In both, space is discretized with a sixth-order centered scheme and the direct numerical integration uses an explicit fourth order Runge Kutta method with fixed time step of $\Delta t = 10^{-2}$ to approximate the temporal derivative. Periodic conditions are used at each boundary of the domain whose length is $L = 100$, using a mesh of 512 points. Numerical integrations with 1024 points have also been performed and showed similar results.

3.1 Results along path 1 ($\theta = 0.6, F$)

Before going any further on the application of the continuation method along *path 1*, let us observe the evolution of the stationary Turing pattern. In Figure 1b, the result of successive numerical integrations of (2) is presented. We observe that the changes of the wavenumber of the pattern are discontinuous. Far from the threshold, the state becomes unsteady and loses its spatial regularity simultaneously, entering a complex dynamical regime whose characterization is out of the scope of this work. Some attempts have been made to understand this scenario [12]. Here we apply the pseudo arc-length continuation method detailed above, starting from the trivial homogeneous solution

$F = R = S = 0$ and increasing F . The output then consists of the modulus of the spatial average $|\langle \Psi \rangle_x| = |\langle \psi \rangle_x|$ of the solution and an integer number $n_p = L/\lambda_0$, where λ_0 is the wavenumber of the pattern under continuation. Figure 2a exhibits the result of these calculations. The main feature of this figure is the multiplicity of possible patterned solutions supported by the system. In addition, the continuation is also able to capture the stability of the branches found. The stability range of each branch is drawn as a solid red curve bounded by two symbols which represent the points where a bifurcation takes place (\square symbols for a stationary bifurcation and \diamond symbols for a Hopf bifurcation). The numerical integration of the LL equation (2) along *path 1* (\triangleright of Fig. 2a) shows the selection of one pattern, which changes its wavelength only sporadically and in a discontinuous fashion, as observed in Figure 1b.

The numerical continuation reveals the richness exhibited by the spatial system. First, for F lower than the critical value given by (6), only the homogeneous equilibrium exists. Second, after the critical value, a bifurcation takes place giving birth to a patterned solution. Further increasing of the forcing repeats this process, giving rise to several other branches of patterned solutions. All but the first branch are unstable when they emerge from the homogeneous branch. The continuation of the branches for larger values of F leads to their stabilization via a stationary bifurcation (represented by \square symbols in Fig. 2a). The resemblance between this scenario and the Eckhaus instability [14,15] is evident. The Eckhaus instability consists of a discrete jump in the wavelength of a stationary solution (spatially periodic) when the control parameter is varied. In our study, all the bifurcations between two different periodic patterns appear to be of the Eckhaus type, hence we will call them indifferently stationary or Eckhaus bifurcations.

The branches of stationary patterns with the largest wavenumbers lose their stability through a Hopf bifurcation. Interestingly this fixes an upper limit for the stationary equilibria. The value of F where dynamical solutions arise is consequently dependent on the branch that was followed before the jump. In Figure 2a we can observe how for $F \approx 2.2$ a Hopf bifurcation destabilizes the last stable branch of stationary patterns. Once the dynamical states have risen, the continuation process used here no longer provides a good description of the dynamics observed.

In addition to representing the solutions by their spatial average, we display the number of wavelengths n_p . In Figure 2b the region of existence for the various branches has been depicted in the (F, n_p) plane. The route along *path 1* followed by the pattern calculated through successive direct integrations of (2) (blue rhombs) shows the correlation between the branches in Figure 2a and their wavelength in Figure 2b.

Experimental optical observations [26] suggest that the wavelength depends continuously on the parameter instead of undergoing finite jumps at discrete locations. In order to understand this, we note that these experiments generally contain a huge number of wavelengths, and

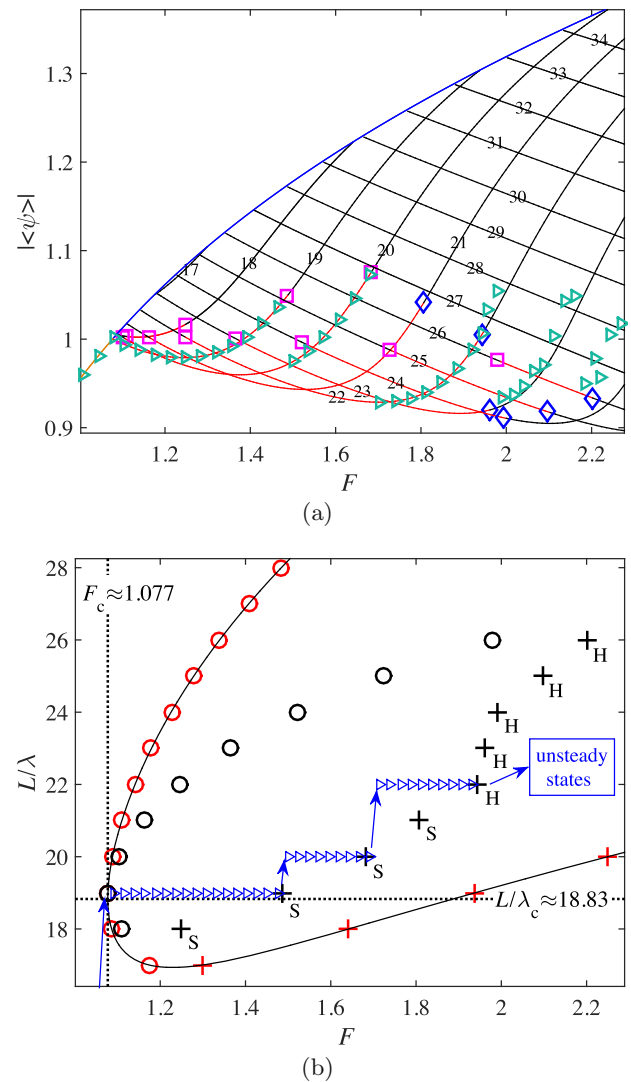


Fig. 2. (a) Continuation of the steady solutions as a function of F : all the branches presented are stationary. The primary branch corresponds to the homogeneous solution and is orange/blue when stable/unstable. The rest of the branches correspond to stationary solutions differentiated from each other by their periodicity n_p noted over each branch. The stable branches have been plotted in red and the unstable ones in black. The changes of stability take place through stationary or Hopf bifurcations, represented by the \square and \diamond symbols respectively. The \triangleright symbols represent results of direct numerical integration following a route up. (b) Intervals of existence (red symbols for pseudo arc-length continuation results, black line for theory) and stability (black symbols) of the branches of periodic patterns as a function of their wavelength. In this representation, the branches are all the horizontal lines of equation $L/\lambda = n_p (n_p \in \mathbb{N})$ lying inside the tongue. The symbols \circ represent the value of F at which a branch begins its existence (red) or stabilizes (black). The $+$ symbols represent points where a branch destabilizes (black) and disappears (red for continuation results, black line for theory). The letters S and H next to the destabilization points signify that the transition occurs through a stationary or a Hopf bifurcation, respectively. The \triangleright symbols show which branch of solutions is followed during the route up as in (a).

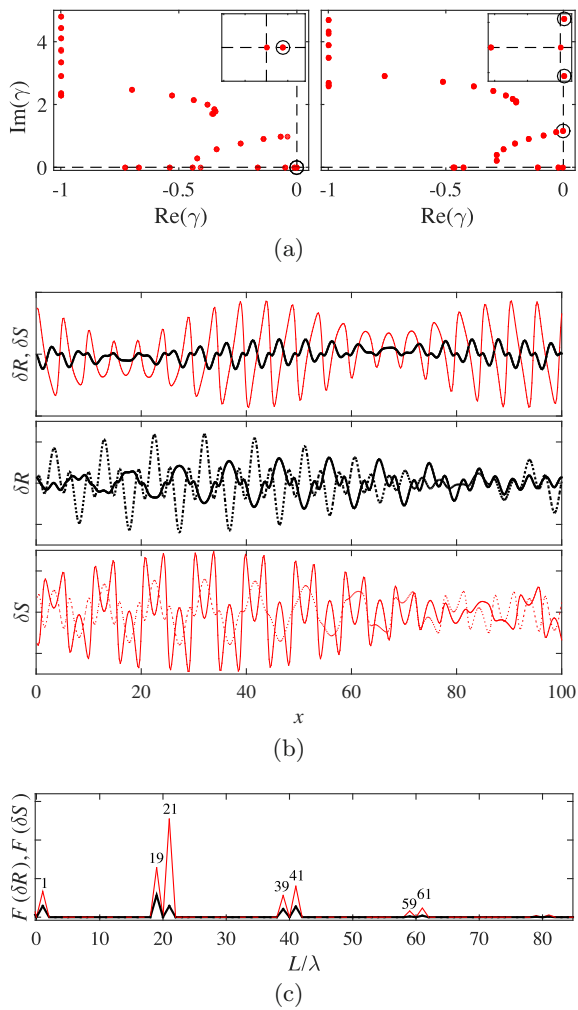


Fig. 3. (a) Part of the spectrum of the Jacobian at the bifurcations where the branches $n_p = 20$ (on the left, stationary bifurcation) and $n_p = 21$ (on the right, Hopf bifurcation) become unstable. The spectrum is symmetric about the real axis and so the eigenvalues with a negative imaginary part are not shown. Insets: zoom at $\Re(\gamma) = 0$. (b) Destabilizing eigenmode $(\delta R, \delta S)$ at the same bifurcations as shown in (a). Top: for $n_p = 20$, δR (in black) and δS are both real. Middle plot: real (solid line) and imaginary (dots) part of δR on the branch $n_p = 21$ at the bifurcation. Bottom: real (solid line) and imaginary (dots) part of δS at the same location. Since eigenvectors are defined up to a constant, the vertical axis ticks have been removed. The middle and bottom plots have the same scaling. (c) Norm of Fourier transform of eigenvector shown in (b) (top), associated with $n_p = 20$, with same conventions for colors. The numbers above each peak indicate its wavenumber.

hence the effects of discretization are far less noticeable than in our simulations, whose domains contain a much smaller number of wavelengths. A change in wavenumber takes place each time the parameter is varied, even slightly, which gives the impression of continuous alteration of the light frequency inside the experimental device.

The set of eigenvalues γ at the transitions on the branches $n_p = 20$ (stationary bifurcation) and $n_p = 21$ (Hopf bifurcation) are compared in Figure 3a, as well as the

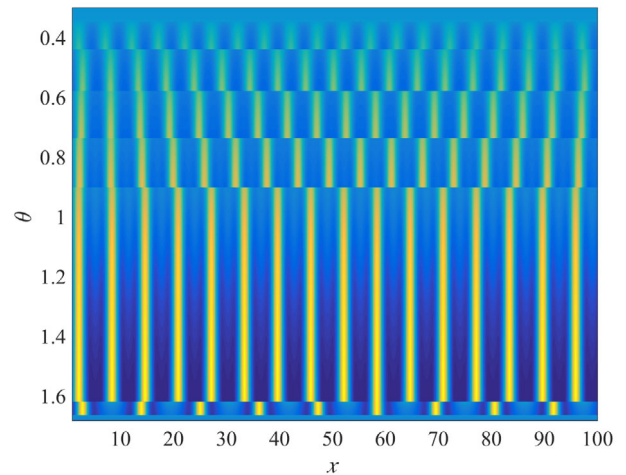


Fig. 4. Contour plot of $|\psi(x, t_*)|$ at $t_* = 10000$ of the states observed from direct numerical integration in the space (horizontal line) at $F = 1.2$ (path 2) and for decreasing θ (see also \triangleleft symbols in Fig. 5).

destabilizing eigenfunction in Figure 3b. The neutral mode of eigenvalue $\gamma_G = 0$ on the spectra of Figure 3a is the Goldstone mode, associated with the translational symmetry of the LL model broken by the pattern. This mode is present on all stationary branches and remains constant as long as these branches exist. The mode responsible for the transitions is never the Goldstone mode but that related to the eigenvalues traversing the imaginary axis rightwards, surrounded by black circles in Figure 3a. The destabilizing mode in Figure 3b contains two distinct scales: a small scale comparable to the wavelength of the pattern and a larger one that modulates the mode. The Fourier transform of the destabilizing mode on the branch $n_p = 20$ (Fig. 3c) indeed exhibits isolated peaks at the spatial frequencies $L/\lambda = \pm 1, \pm 19, \pm 21, \pm 39, \pm 41, \dots$. This feature seems to be shared by the critical eigenmodes at each stationary bifurcation in Figure 2 (\square symbols): the mode destabilizing the branch n_p contains exclusively the low wavenumber $L/\lambda = 1$, the larger ones $n_p \pm 1, 2n_p \pm 1, \dots$ and their negative counterparts. This is characteristic of the Eckhaus instability.

Comparison with the direct integration suggests that the low wavenumber of the destabilizing mode is correlated with the jump of wavenumber only at the lowest values of F (see Fig. 2 where the solution jumps directly from $n_p = 20$ to $n_p = 22$). Similar results have been reported in other contexts like experimental electroconvection [27] or numerical simulation of Taylor vortices [28] and are henceforth not surprising. The type of bifurcation changes (stationary \rightarrow Hopf) when the marginal eigenvalues (as well as the corresponding eigenvector) become complex (see Figs. 3a and 3b), inducing oscillatory dynamics.

3.2 Results along path 2 ($\theta, F = 1.2$)

The same study is carried out along the path where only the detuning θ varies, with a constant $F = 1.2$. In Figure 4,

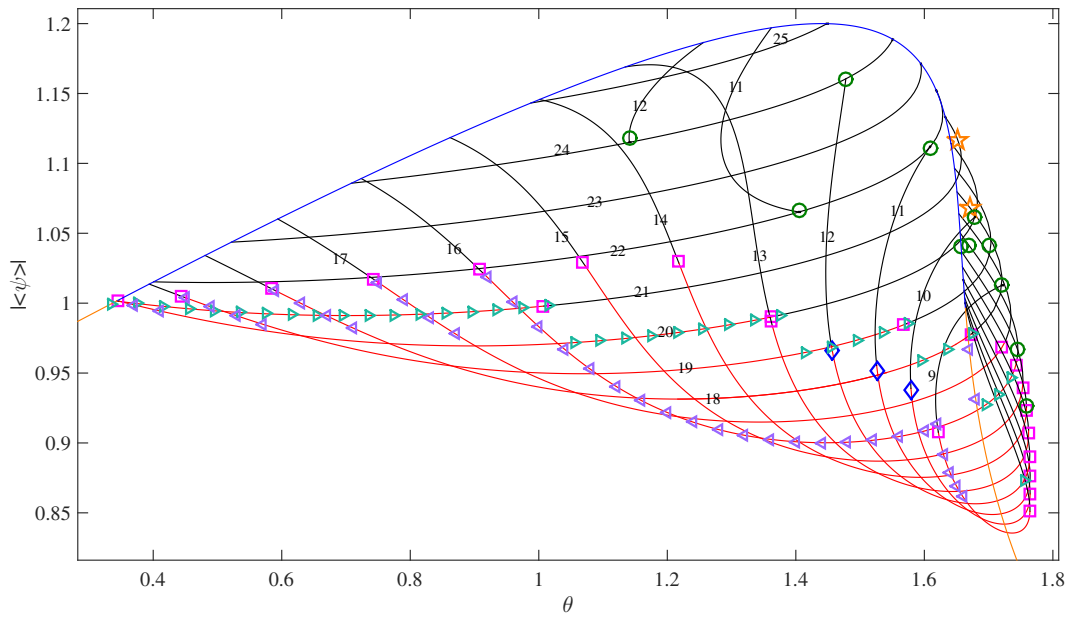


Fig. 5. Part of the bifurcation diagram over *path 2* ($\theta, F = 1.2$). Same conventions as in Figure 2. In addition, period-doubling and period-tripling branching points are observed, denoted by green \circ and orange \star , respectively. Two direct numerical integrations have been conducted: by increasing θ (\triangleright symbols) and by decreasing θ (\triangleleft symbols). This plot displays all the branches of highest wavenumbers and those which eventually become stable to make the comparison between simulation and continuation easier. The remaining branches are represented in Figure 6.

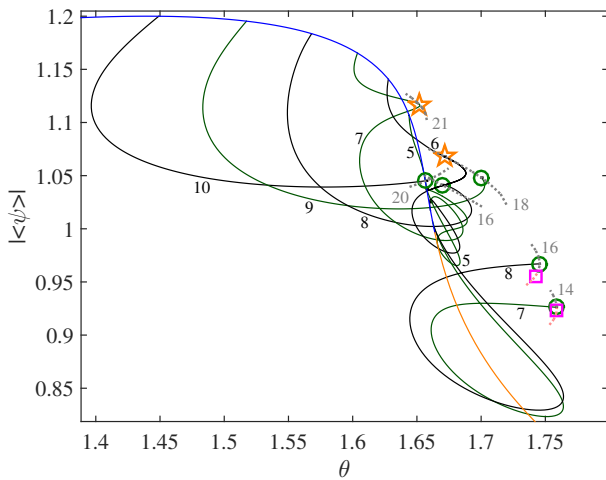


Fig. 6. Part of the bifurcation diagram over *path 2* ($\theta, F = 1.2$) that completes Figure 5. The plot shows the branches of low wavenumber which are all unstable. They have been plotted in black (n_p even) and dark green (n_p odd) to make them easier to follow. Portions of the branches of Figure 5 emanating from the branching points (\circ and \star) appear here with dotted gray or pink lines according to their stability.

the patterns remain stationary all along the chosen θ range and are homogeneous at *both* endpoints of the θ range.

As for *path 1*, we compare the results of the numerical integration with those of the continuation in the bifurcation diagram presented in Figures 5 and 6. The diagram has been split into two for the sake of legibility. The bifurcation diagram obtained in Figures 5 and 6 exhibits many

similarities with its counterpart along *path 1* (Eckhaus bifurcations, multistability, Hopf bifurcations leading to unsteady states) but fundamental differences need also to be mentioned. The homogeneous branch destabilizes at a second threshold $\theta \approx 1.664$, where the bifurcation is subcritical and multi stability is observed between the homogeneous state and stationary patterns. Period-doubling and period-tripling branching points absent from Figure 2a appear in Figures 5 and 6 but they are never located on the stable part of any branch, at least for this value of F . For this reason we name them branching points, not bifurcations. We also observe that the period-doubling points always terminate the branch with long (double) wavelength. In contrast, the long (triple) wavelength branch is continued at each side of the period-tripling branching point. In fact, the continuation method shows that at the period-doubling branching points the solution travels back the long-wavelength branch taking the shape of a pattern which is translated by half a wavelength in comparison to the solution travelling forth the branch, as shown in Figure 7 left. Both solutions are exactly equivalent and consequently they have the same norm $|\langle \psi \rangle_x|$. In contrast, continuing a branch further period-tripling points leads to other solutions that cannot be superposed to the initial ones up to a translation (see Fig. 7 left, at each side of the dotted line). These results suggest that the period-doubling branching points would support pitchfork bifurcations, whereas the period-tripling branching points would be associated to transcritical bifurcations. Also, the branches characterized by the wavenumbers $n_p \in [5, 12]$ appear at two distinct locations, which was not the case over *path 1*. Again, the direct integrations (both upwards

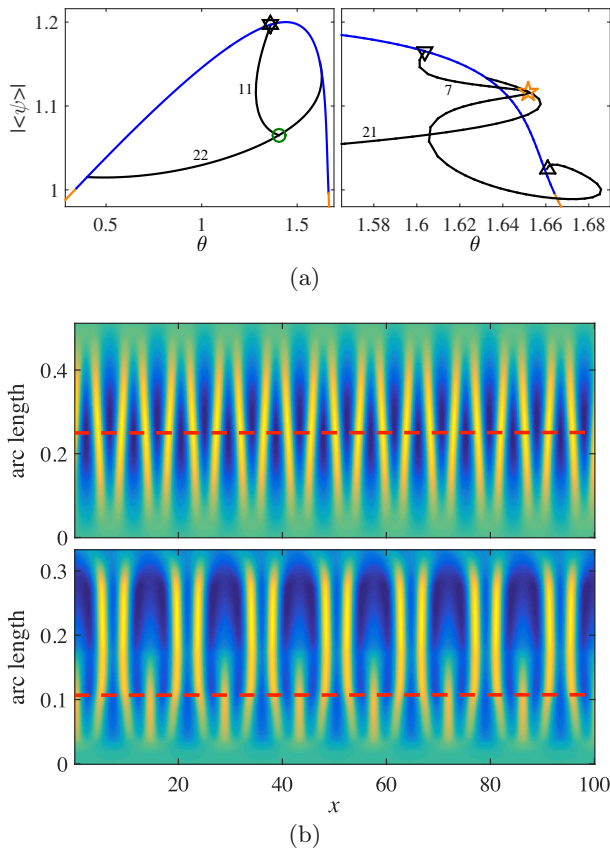


Fig. 7. (a) Special branches of Figures 5 and 6 associated with a period-doubling ($n_p = 11$, left) and a period-tripling ($n_p = 7$, right) branching point. (b) Corresponding space-arc-length diagrams following the branches $n_p = 7$ (top) and $n_p = 11$ (bottom). The period-doubling and period-tripling point positions are highlighted by the dashed red lines. The minimal and maximal arc lengths correspond to the points shown as symbol ∇ and symbol Δ , respectively, in (a).

and downwards) lend support to the results stemming from the continuation.

4 Analytical prediction of the Eckhaus instability

The aim of this section is to provide an analytic interpretation to the wavenumber selection process observed by the continuation technique. For this purpose we use the same strategy as in [12]. The first stage consists of the derivation of the order parameter equation governing the dynamical behavior in the weakly nonlinear regime, which will be used to study the Eckhaus instability, leading to the determination of the selected wavenumber. Following the guidelines of [15], the whole analysis is performed on the equation which governs the dynamics of the amplitude A of the patterns. These patterns are approximated by (7) according to the linear analysis. The amplitude equation can be derived in the vicinity of the instability by means of a weakly nonlinear analysis. We use a normal

form procedure [6,29]. Since this amplitude equation is derived from (3) and admits solutions of the form (7), it must be phase-invariant and possess the symmetry $x \rightarrow -x$. Hence, we know a priori that the equation will have the form

$$\partial_t A = \phi C_1 A + C_3 |A|^2 A + C_s \partial_{xx} A, \quad (8)$$

where all the coefficients C are real and $\phi \ll 1$ represents the small deviation of the control parameter from the critical point. In this section we use F as our control parameter, the critical value is given by (6).

In order to compute the spatial derivatives, we have assumed the existence of two spatial scales (one for the pattern and a slower one for the amplitude). We carry out the aforementioned analysis by setting the following change of variables:

$$(R, S) = (R_h, S_h)_c + \mathbf{U}^{[1,0,0]} + \mathbf{U}^{[2,0,0]} + \dots + \mathbf{U}^{[1,1,0]} + \dots + \mathbf{U}^{[1,0,1]} + \mathbf{U}^{[1,0,2]} + \dots \quad (9)$$

where $(R_h, S_h)_c$ is the homogeneous solution at the critical point and the right hand side of this expression corresponds to a polynomial series in 3 variables $[m, n, p]$ standing for the orders of the amplitude, the unfolding parameter and the spatial derivatives ($[O(|A|^m), O(\phi^n), \partial_x^p]$) respectively. Substituting (9) into (3), setting $F = F_c + \phi$ and solving this problem order by order, we find the coefficients

$$C_1 = 2 \frac{F_c}{(\theta - 2)^2}, \quad C_s = 2(2 - \theta),$$

$$C_3 = \frac{4(30\theta - 41)F_c^2}{9(\theta^2 - 2)^2}. \quad (10)$$

These coefficients are in good agreement with previous observations [7,16]. At $(\theta_{cd2} = 41/30, F_c(\theta_{cd2}))$ C_3 vanishes, leading to a co-dimension 2 point where the bifurcation passes from sub- to super-critical. In the particular case of the *path 1*, the bifurcation is super-critical ($C_3 < 0$) and takes place in the direction of increasing forcing ($C_1 > 0$).

All the terms involved in (8) must be of the same order to play a significant role in the dynamics. Hence, the following scaling laws must be satisfied

$$A \sim \phi^{1/2}, \partial_t \sim \phi \sim \partial_{xx}. \quad (11)$$

Moreover, defining

$$\tau = |C_3|t, \quad \xi = \sqrt{\frac{|C_3|x}{C_s}}, \quad (12)$$

equation (8) becomes the Ginzburg-Landau equation

$$\partial_\tau A' = \mu A' + \text{sign}(C_3) |A'|^2 A' + \partial_{\xi\xi} A', \quad (13)$$

where $A'(\tau, \xi) = A(t, x)$ and $\mu = \phi C_1 / |C_3|$. At $\theta = 0.6$, $\text{sign}(C_3) = -1$ and then we can directly apply the analysis of [15] to predict the values of F where new branches appear and stabilize. These predictions should work as long as (8) describes the amplitude.

In the following, we use three results of [15] applied to our case. In order to be clear and concise, we present the same equation containing first the results for (13) and then their counterpart that matches with (8).

First, there exists a family of patterns born unstable and in a super-critical way from the homogeneous branch. In a domain of size L' , these patterns have a wavelength $k' = k'_c + Q'$ where k'_c is the critical wavenumber of the infinite system (13) and Q' is such that $k' = 2l\pi/L'$, $l \in \mathbb{Z}$ (the prime is associated to the rescaled system (13); the same variables without primes are linked with the LL model). Such a branch appears at

$$\mu_l = \frac{C_1}{|C_3|} \phi = Q'^2, \quad F_l = F_c + \frac{C_s}{C_1} \left(\frac{2\pi l}{L} - k_c \right)^2. \quad (14)$$

Second, given an integer l and the associated number Q' , a branch becomes stable at:

$$\begin{aligned} \mu_{l,stab} &= 3Q'^2 - \left(\frac{\pi}{L'} \right)^2, \\ F_{l,stab} &= F_c + \frac{C_s}{C_1} \left(3 \left(\frac{2\pi l}{L} - k_c \right)^2 - \frac{1}{2} \left(\frac{2\pi}{L} \right)^2 \right). \end{aligned} \quad (15)$$

Finally, given an integer l and the associated number Q' , a branch has an amplitude given by

$$A'_l = \sqrt{\mu - Q'^2}, \quad A_l = \sqrt{\frac{-\phi C_1 + C_s Q^2}{C_3}}. \quad (16)$$

The estimates for F_l from (14) and $F_{l,stab}$ from (15) for the Ginzburg-Landau equation are compared with our numerical results for the LL model in Figure 8a.

We compare the amplitude of the patterns obtained from LL with the amplitudes stemming from the normal form. The results are shown in Figure 8b. We deduce A from the norm of a given simulated pattern l by taking its Discrete Fourier Transform with respect to x , extracting the component of wavenumber $k = k_c + Q$ from the series and dividing it by $\|\mathbf{w}\|$ (see Eq. (7)). It seems that the results for A from the Ginzburg-Landau equation and from the simulations of the LL equation fit well close to the threshold. Nonetheless, they move rapidly apart from each other.

The Ginzburg-Landau equation (8) is used to approximate the LL model (2) near F_c , but it possesses properties that are not shared by (2). First, solutions of (8) characterized by the wavenumbers $k_c + Q$ and $k_c - Q$ have the same amplitude according to (8). Second, the branches of solutions of (8) are all parabolas; thus for a fixed wavenumber, A should be a monotonically increasing function of ϕ . In contrast, our numerical calculations show that there is a strong asymmetry between the patterned solutions of wavenumbers $k < k_c$ and $k > k_c$ in the

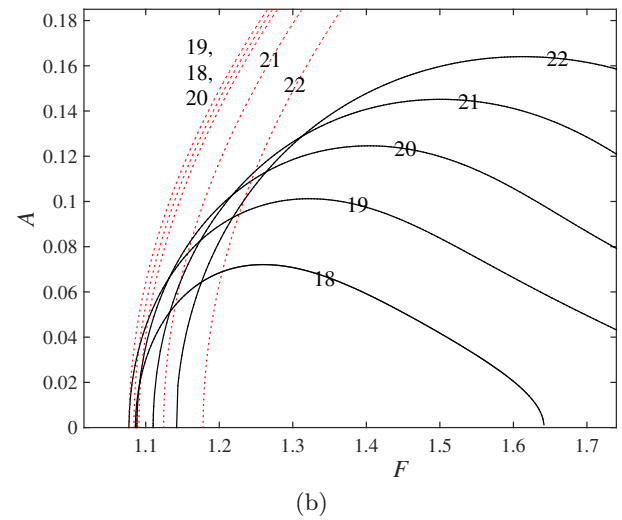
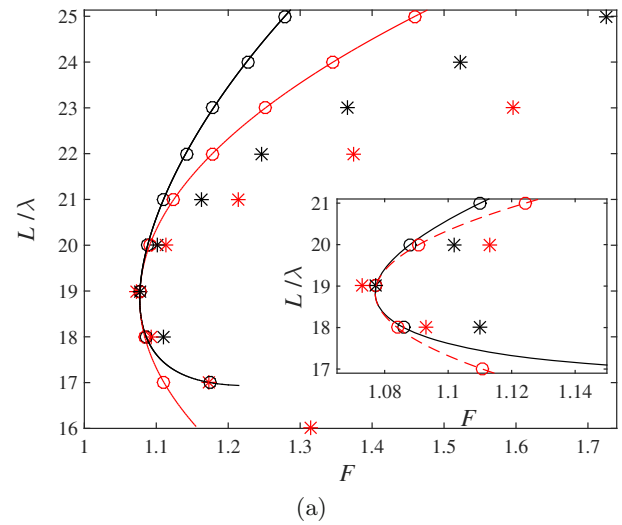


Fig. 8. (a) Values of F_l (\circ and lines) and $F_{l,stab}$ ($*$) for each branch n_p . Comparison between the simulated LL model (black symbols, same as \circ in Fig. 2b) and its Ginzburg-Landau approximation (red symbols, see Eqs. (14) and (15)). (b) Amplitude of the pattern A as a function of F . Comparison between the branches of the Ginzburg-Landau approximation (red dashed curves, see (16)) and the LL model (black lines). All branches are labelled by their n_p value.

LL model (2). In (2), the patterned branches terminate on the homogeneous state if F is sufficiently increased, as shown in Figure 8b. We even observe that the real part R of the solutions of (2) undergoes a rapid change of sign, which implies that A is better approximated computing it from S than from R . The branches of solutions of (2) for wavenumbers lower than k_c return very early towards the homogeneous branch. As a result, they present worse agreement than their counterparts with $k > k_c$. These qualitative differences between the solutions of the LL model and those of the normal form approximation may disappear if terms with higher powers of $|A|$ and higher derivatives ∂_x^p are included in the normal form. Finally, note that the value of stabilization of the branches

according to the Ginzburg-Landau model (red stars in Fig. 8) is slightly below the marginal curve of the LL equations (black line) for $n_p \in [17, 19]$, and hence is not meaningful since a branch cannot undergo a bifurcation when it does not yet exist. At the threshold, $n_p = 19$, this phenomenon is characteristic of the Eckhaus instability in finite domains and has been discovered in [15]. Here, the same phenomenon occurs at $n_p = 17$ and $n_p = 18$; its cause is the asymmetry of the LL model with respect to k_c .

5 Discussion

The aim of our investigation was to describe the successive bifurcations undergone by a solution of (2) before it became unsteady. In this direction, the continuation provided a cobweb that consists of numerous branches of static solutions each characterized by its wavenumber. The transitions between these branches occurs through Eckhaus instabilities as the parameter is changed. Eckhaus instabilities have been reported in similar systems (e.g. [30]). Dynamical states arise after one of these branches destabilizes through a Hopf bifurcation. This phenomenon occurs at large F values. These results have important implications. Given the length of the system, we can predict numerically where the transition between branches will take place as well as the upper limit for the stability of the stationary states. Besides, by moving back and forth the control parameter it must be possible to control the wavenumber following the various paths in the cobweb (cf. Fig. 2a) of branches. These numerical predictions can be investigated experimentally. Furthermore, the coexistence of several stable branches suggests the possible presence of mixed modes [31] (fronts connecting patterns with two distinct wave-numbers). These features can be the subject of a future investigation.

The amplitude equation (8) describes the dynamics only locally and does not account for the temporal oscillations. In order to present oscillations the coefficients C in (8) should be allowed to be complex, but this would violate the symmetries inherited from (2). Consequently, we know the normal form will work quantitatively in the vicinity of the instability (it matches the first three instabilities (cf. Fig. 8a)) but only qualitatively as we go away from the instability, and eventually deviates entirely from the behavior of the L-L equation. Since the normal form fails to predict the Hopf bifurcations, proposing an amended equation is an open question.

As a final remark, the dynamical states emerge due to a Hopf bifurcation and it is therefore natural to assume that these oscillations will play a fundamental role in the complex dynamics observed for larger values of the forcing. Actually, in [32] quasiperiodicity has been proposed as the route towards chaos. This has been studied [33] in a system which displays essentially the same features as (2), including an Eckhaus scenario. For these reasons, the most intriguing open question is whether the mechanism of destabilisation, which starts with an Eckhaus scenario followed by a Hopf bifurcation and the later appear-

ance of several frequencies ending in a spatio-temporal chaotic behaviour, is the right route in this system. If the route is the same here as in [33], then it is possible to propose that it is a robust mechanism for destabilisation of extended systems in nature.

The authors thank L.S. Tuckerman, M. Tlidi, M. Clerc, C. Falcón and A. Champneys for very fruitful discussions. N. Verschuere acknowledges Programa de doctorado en el Extranjero Becas Chile Contract No. 72130186. N. Perinet acknowledges the financial support of FONDECYT, postdoctorate project 3140522. The simulations were done using the supercomputer Lefraru of the NLHPC facility.

Author contribution statement

All the authors worked on the theoretical description and discussed the results. N.P. developed the codes and performed the direct numerical simulations as well as the continuation. N.V. and N.P. performed the analytical calculations (Linear stability analysis and normal form). All the authors were involved in the writing of the last version of the manuscript. Most of the figures were created by N.P.

References

1. M. Haelterman, S. Trillo, S. Wabnitz, *Opt. Commun.* **91**, 401 (1992)
2. P. Kockaert, P. Tassin, G. Van der Sande, I. Veretennicoff, M. Tlidi, *Phys. Rev. A* **74**, 033822 (2006)
3. L. Gelens, G. Van der Sande, P. Tassin, M. Tlidi, P. Kockaert, D. Gomila, I. Veretennicoff, J. Danckaert, *Phys. Rev. A* **75**, 063812 (2007)
4. Y.K. Chembo, N. Yu, *Phys. Rev. A* **82**, 033801 (2010)
5. J. Ye, T.W. Lynn, *Adv. At. Mol. Opt. Phys.* **49**, 1 (2003)
6. M. Haragus, G. Iooss, *Local Bifurcations, Center Manifolds, and Normal Forms in Infinite-Dimensional Dynamical Systems* (Springer, 2011)
7. L.A. Lugiato, R. Lefever, *Phys. Rev. Lett.* **58**, 2209 (1987)
8. P. Mandel, M. Tlidi, *J. Opt. B: Quantum Semiclassical Opt.* **6**, R60 (2004)
9. S. Coulibaly, M. Taki, M. Tlidi, *Opt. Exp.* **22**, 483 (2014)
10. W.J. Firth, A.J. Scroggie, G.S. McDonald, L.A. Lugiato, *Phys. Rev. A* **46**, R3609(R) (1992)
11. M. Tlidi, R. Lefever, P. Mandel, *Quantum Semiclassical Opt.: J. Eur. Opt. Soc. B* **8**, 931 (1996)
12. Z. Liu, F. Leo, S. Coulibaly, M. Taki, *Phys. Rev. A* **90**, 033837 (2014)
13. C. Godey, I.V. Balakireva, A. Coillet, Y.K. Chembo, *Phys. Rev. A* **89**, 063814 (2014)
14. W. Eckhaus, *Studies in Nonlinear Stability Theory* (Springer-Verlag, Berlin, Germany, 1965)
15. L.S. Tuckerman, D. Barkley, *Physica D* **46**, 57 (1990)
16. D. Gomila, A.J. Scroggie, W.J. Firth, *Physica D* **227**, 70 (2007)
17. P. Parra-Rivas, D. Gomila, M.A. Matías, S. Coen, L. Gelens, *Phys. Rev. A* **89**, 043813 (2014)
18. P. Parra-Rivas, D. Gomila, E. Knobloch, S. Coen, L. Gelens, *Opt. Lett.* **41**, 2402 (2016)

19. P. Parra-Rivas, E. Knobloch, D. Gomila, L. Gelens, Phys. Rev. A **93**, 063839 (2016)
20. E. Allgower, K. Georg, *Introduction to Numerical Continuation Methods* (Society for Industrial and Applied Mathematics, 2003)
21. W.J.F. Govaerts, *Numerical Methods for Bifurcations of Dynamical Equilibria* (Society for Industrial and Applied Mathematics, Philadelphia, PA, 2000)
22. H.A. Dijkstra, F.W. Wubs, A.K. Cliffe, E. Doedel, I.F. Dragomirescu, B. Eckhardt, A.Y. Gelfgat, A.L. Hazel, V. Lucarini, A.G. Salinger, E.T. Phipps, J. Sanchez-Umbria, H. Schuttelaars, L.S. Tuckerman, U. Thiele, Commun. Comput. Phys. **15**, 1 (2014)
23. Y. Kuznetsov, *Elements of Applied Bifurcation Theory* (Springer-Verlag, Berlin, Germany, 2004)
24. F. Schilder, H.M. Osinga, W. Vogt, SIAM J. Appl. Dyn. Syst. **4**, 459 (2005)
25. E.J. Doedel, M.J. Friedman, J. Comput. Appl. Math. **26**, 155 (1989)
26. S. Coulibaly, M. Taki, A. Bendahmane, G. Millot, B. Kibler, M.G. Clerc, private communication
27. M. Lowe, J. Gollub, Phys. Rev. Lett. **55**, 2575 (1985)
28. H. Riecke, H.G. Paap, Phys. Rev. A **33**, 547 (1986)
29. C. Elphick, E. Tirapegui, M. Brachet, P. Coulet, G. Iooss, Physica D **29**, 95 (1987)
30. A. Bergeon, J. Burke, E. Knobloch, I. Mercader, Phys. Rev. E **78**, 046201 (2008)
31. U. Bortolozzo, M.G. Clerc, C. Falcon, S. Residori, R. Rojas, Phys. Rev. Lett. **96**, 214501 (2006)
32. D. Gomila, P. Colet, Phys. Rev. A **68**, 011801 (2003)
33. M.G. Clerc, N. Verschueren, Phys. Rev. E **88**, 052916 (2013)